Correlation between the morphology of cobalt oxalate precursors and the microstructure of metal cobalt powders and compacts

V. Baco-Carles *, A. Arnal, D. Poquillon, Ph. Tailhades

Institut Carnot CIRIMAT, UMR CNRS 5085, Université Paul Sabatier, 118 Route de Narbonne, 31062 Toulouse cedex 09, France

Abstract

Metal cobalt powders of well-controlled size and morphology were synthesized by thermal decomposition under hydrogen of precipitated cobalt oxalates. Green compacts were prepared by uniaxial pressing of metal powders at 290 MPa. The bending green strength of the metal compacts was measured.

A precipitation from ammonium oxalate and oxalic acid gives rise to the formation of β-$CoC_2O_4 \cdot 2H_2O$ particles of parallelepipedic and acicular morphology, respectively. An increase in the length to diameter ratio of the precursor particles favours an entanglement of the elementary grains during the thermal decomposition. Therefore, irregular and rough metal particles have been obtained. This specific morphology favours a mechanical interlocking of the particles during the compaction, leading to high values of green density and green strength of the metal compacts.

Keywords: Cobalt powder; Oxalate; Porous metals; Particles morphology; Green compact; Green strength

1. Introduction

Metal cobalt powders have many applications, notably in steels for cutting tools, abrasion strengthened composites [1,2] and also, in alkaline rechargeable batteries [3] or heterogeneous catalysis [4]. The mechanical performances of the final materials closely depend on the quality of the green powder compacts. In particular, the compacted metal pieces must outlive ejection from the die and allow handling before subsequent processing, such as sintering or hot extrusion. Whereas several authors have studied the influence of spherical metal powder granulometry on the green strength of pressed powder compacts [5–8], few [9] deal with the effect of the metal particles shape. Previous works [10,11] have revealed that a coralline shape of metal iron particles gives rise to an exceptional value for the metal compact green strength (60 MPa for a compaction pressure of 290 MPa). The preparation process leading to these particles is based on the thermal decomposition under hydrogen of precipitated oxalic precursors of well-controlled morphology. Thus, it has been shown that an acicular shape of the ferrous oxalate particles induces, after reduction into metal iron, an entanglement of the elementary grains giving rise to a coralline shape. It is assumed that this specific morphology, characterized by an important intragranular porosity, allows a strong overlapping of the adjacent filamentous grains during the compaction. As a result, a rigid metallic skeleton was formed and an outstanding value of bending green strength was obtained.

The chemical parameters of the synthesis permitting to obtain metal cobalt particles with a coralline shape are presented in this work. The influence of the morphology of the cobalt oxalate particles on both the microstructure of the metal cobalt powders and the corresponding compacts is studied. Values of the bending green strength obtained for the compacts are then discussed.

2. Experimental

2.1. Chemical synthesis

2.1.1. Oxalate powders

Six oxalate powders were prepared according to the chemical procedure described thereafter. The oxalate powders

* Corresponding author.
E-mail address: baco@chimie.ups-tlse.fr (V. Baco-Carles).

doi:10.1016/j.powtec.2007.10.016

Table 1
Chemical parameters used for the synthesis of the cobalt oxalate powders

Oxalate powder	Cobalt salt	Oxalate salt	Addition flow (L h^{-1})
OXA1	$CoCl_2{\cdot}6H_2O$ (0.20 mol L^{-1})	$H_2C_2O_4{\cdot}2H_2O$ (0.20 mol L^{-1})	2.7
OXA2	$CoCl_2{\cdot}6H_2O$ (0.50 mol L^{-1})	$H_2C_2O_4{\cdot}2H_2O$ (1.33 mol L^{-1})	2.4
OXA3	$CoCl_2{\cdot}6H_2O$ (1.00 mol L^{-1})	$H_2C_2O_4{\cdot}2H_2O$ (1.33 mol L^{-1})	1.2
OXA4	$Co(NO_3)_2{\cdot}6H_2O$ (2.86 mol L^{-1})	$H_2C_2O_4{\cdot}2H_2O$ (1.33 mol L^{-1})	1.0
OXA5	$CoSO_4{\cdot}7H_2O$ (2.00 mol L^{-1})	$H_2C_2O4{\cdot}2H_2O$ (0.20 mol L^{-1})	1.5
OXO6	$CoCl_2{\cdot}6H_2O$ (2.20 mol L^{-1})	$(NH_4)_2C_2O_4{\cdot}H_2O$ (0.17 mol L^{-1})	1.6

are hereinafter referred to as OXA1, OXA2, OXA3, OXA4, OXA5 when cobalt ions were precipitated from oxalic acid and OXO6 when cobalt ions were precipitated from ammonium oxalate. The chemical parameters used for the six oxalates are presented in Table 1. A cobalt salt was dissolved at 20 °C in deionised water. This solution was added to an aqueous solution of an oxalate salt kept at 20 °C. The precipitated oxalate was separated by filtration after 15 min, washed with deionised water, and dried out at 80 °C. The oxalate powder was finally deagglomerated by simply sieving through a 250 μm sieve.

2.1.2. Metal cobalt powders and compacts

The oxalate powders were reduced at 520 °C under dry hydrogen during 2 h. The so-obtained metal cobalt powders were deagglomerated by simply sieving through a 250 μm sieve. These powders are hereinafter referred to as OXA1R, OXA2R, OXA3R, OXA4R, OXA5R and OXO6R, respectively.

Whatever the studied sample is, an equivalent quantity of 6 g of powder was further compacted at 20 °C using a SPECAC uniaxial hydraulic press. As only the lower punch of the apparatus could move, single-end pressing was carried out. The conversion of the hydraulic pressure into a force imposed to the lower punch is directly read in a gauge. The force transmitted to the upper punch was not measured and the wall friction effects could not be quantified. The compaction pressure was determined considering the force applied on a surface of 12.7 mm in width and 31.8 mm in length. The maximal pressure used was limited to 290 MPa because of the low mechanical properties of both the die and associated punches made of stainless steel. No binder was added to the powders. However, in order to make the ejection of the compacts easier, the die and punch walls were lubricated with zinc stearate suspended in acetone. The metal compacts are hereinafter referred to as OXA1RC, OXA2RC, OXA3RC, OXA4RC, OXA5RC and OXO6RC, respectively.

A typical variation of the density versus the compaction pressure was already reported in a previous paper [12]. Three domains were revealed. Elastic deformations of the particle heap occur during the stage I. The stage II is representative of a particle rearrangement by an interparticle sliding. Stage III starts when a particle interlocking generates plastic deformations which are first localised at the contact areas between the particles.

3. Characterization

Phase detection was carried out by X-ray diffraction (XRD) pattern analysis ($\lambda_{Cuk\alpha}$=0.15418 nm).

The oxidation rate of the metal cobalt powders was determined by thermogravimetric analysis. The method is based on the reduction at 1000 °C under pure hydrogen of CoO (generally located at the surface of the metal particles) to pure Co, according to the following reaction:

$$(1-x)\mathrm{Co} + x\mathrm{CoO} + x\mathrm{H_2} \rightarrow \mathrm{Co} + x\mathrm{H_2O}$$

Considering the mass loss Δm of the sample during the reduction, it follows:

$$\Delta m/m = [\mathrm{M_o}(x)]/[\mathrm{M_{Co}}(1-x) + \mathrm{M_{CoO}}(x)] = 16x/(58.93-16\mathrm{x})$$

where: m is sample mass (g),

Δm is mass loss (g),

$$\mathrm{M_o} = 16\mathrm{gmol^{-1}}, \mathrm{M_{Co}} = 58.93\mathrm{gmol^{-1}}, \mathrm{M_{CoO}} = 74.93\mathrm{gmol^{-1}}.$$

Then: $x=3.68[\Delta m/(m+\Delta m)]$,

And: Percentage of metallic cobalt (wt.%)=100 $[(1-x)\mathrm{M_{Co}}]/[(1-x)\mathrm{M_{Co}}+x\mathrm{M_{CoO}}]$.

The oxalate powders, the metal powders and the surface of the metal compacts were observed by scanning electron microscopy (SEM) using a JEOL JSM 6400 (15 kV accelerating voltage). The particle size was determined on different micrographs. About 30–50 particles were measured to estimate the average size. The specific surface area S_w of the metal powders was measured by the BET method using N_2 adsorption at liquid N_2 temperature. A triplicate test of the angle of repose was performed under the standard AFNOR NF A95–113 to compare the sliding and rearrangement facilities of the metal powders. The cold pressed compacts were subjected to a three point bending test as per the MPIF 15 standard norm [13]. An Adamel Lhomargy DY32 apparatus was used for these measurements. During the test, the compact was centrally located in the transverse rupture fixture and was perpendicular to the supported rods. A uniform load, at a rate of approximately 10 kg min^{-1}, was applied on the top of the compact until it ruptures. For a same specimen, the three point bending test was multiplied three times. A typical graph of the imposed load against the crosshead displacement was already reported in a previous paper [14]. This graph reveals that the macroscopic response of the green compact is elastic.

4. Results and discussion

4.1. Oxalate powders

The analysis of the XRD patterns of the cobalt oxalate powders reveals the presence of the diffraction peaks of β-$CoC_2O_4{\cdot}2H_2O$. Indeed, several authors [15,16] have shown that crystallization can lead to different allotropic forms depending on the precipitation conditions. According to Deyrieux and Peneloux [16],

the stable and metastable forms, respectively noted α and β, have different crystallographic structures and differ from each other by the relative positions of the metal-oxalate chains. Lagier [17] has shown that an excess of ammonium oxalate favours the precipitation of the stable form. On the contrary, the metastable form has generally been obtained by a precipitation from oxalic acid. In our case, the obtained phase is not influenced by the nature of the oxalate source. As shown by Tailhades [18], metastable form stabilization might originate in a small size of the oxalate crystallites.

The morphology of the oxalate particles synthesized from oxalic acid is acicular (Fig. 1a–e). The particles tend to join together to form bundles (Fig. 1f). The precipitation from ammonium oxalate gives rise to the formation of parallelepipedic grains (Fig. 2a) aggregated in largest particles of similar shape (Fig 2b). The apparent density (d_a) of the oxalate powders, the average length (L) and the length to diameter average ratio (L/d) of the particles are presented in Table 2.

The powders prepared from ammonium oxalate present an apparent density higher than those of the powders synthesized from oxalic acid (Table 2). Indeed, the OXO6 particles are characterized by an acicular ratio lower than those of OXAn ($1 \leq n \leq 5$). These particles, more isotropic in shape than the needles, fill most compactly a definite volume (V) during a gravitational flow. On the contrary, an increase in the length and in the acicular ratio of the particles induces a decrease in the apparent density of the powders (Table 2). This phenomenon is explained by a favoured entanglement of the needles during a

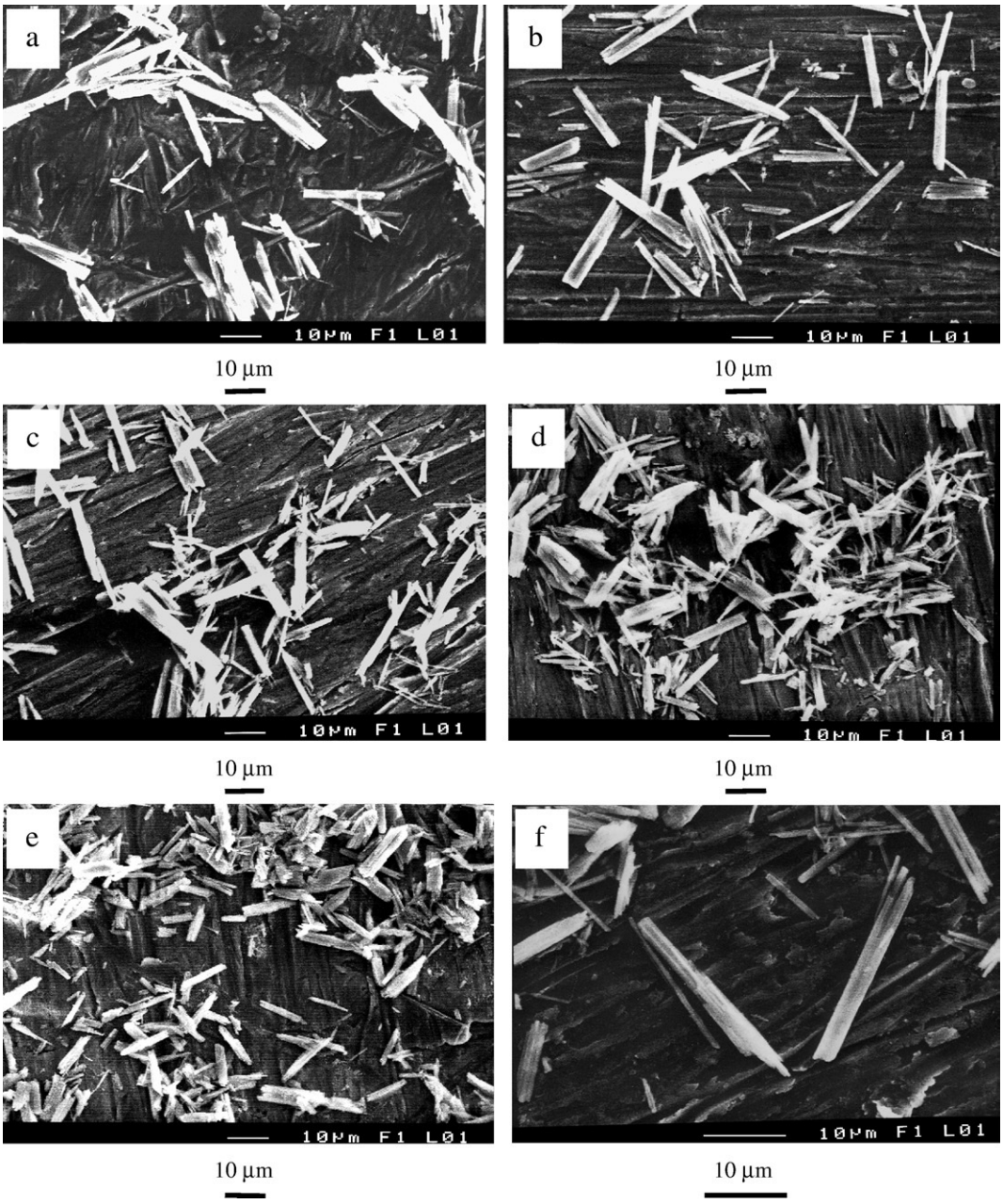

Fig. 1. SEM micrographs of the oxalate precursors: (a) OXA1; (b) OXA2; (c) OXA3; (d) OXA4; (e) OXA5; (f) bundle of acicular particles.

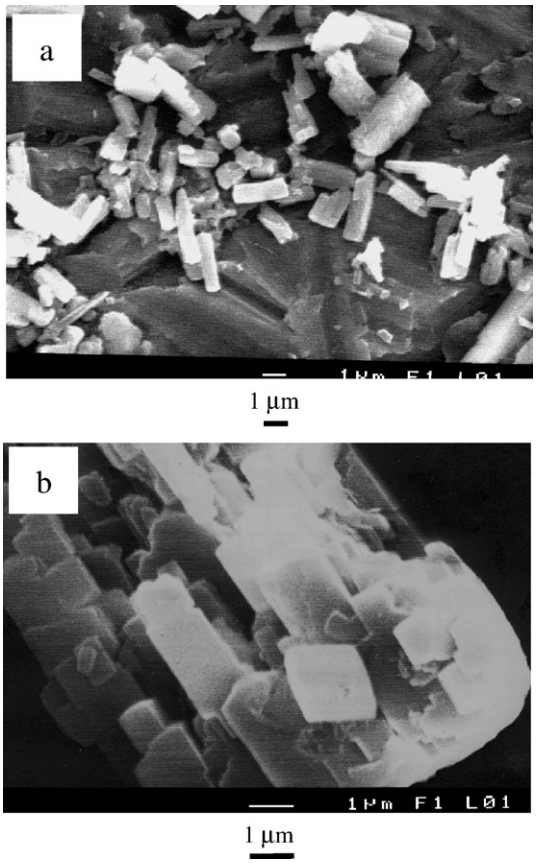

Fig. 2. SEM micrograph of OXO6: (a) primary grains; (b) parallelepipedic particles constituted by an aggregation of the primary grains.

gravitational flow and therefore, by a well spaced out filling of a volume V. It has already been studied by J. G. Parkhouse and A. Kelly [19]. The variation of the apparent density versus the acicular ratio of the oxalate particles fits quite well with the theoretical and experimental curves reported in their paper.

4.2. Metal cobalt powders

For all the powders prepared, XRD analysis reveals the presence of a high proportion of the metastable face centered cubic (fcc) cobalt and a very small proportion of the stable hexagonal close packed (hcp) cobalt. The ratio between the proportion of the metastable and stable phases is the same whatever the studied sample is. The presence of a majority of fcc phase could be explained by a small size of the metal crystallites

Table 2
Characteristics of the oxalate powders

Oxalate Powder	L (±0.5 µm)	L/d	d_a (±0.001 g cm^{-3})
OXA1	17.6	15	0.299
OXA2	16.1	15	0.377
OXA3	13.3	7.7	0.395
OXA4	11.2	6.8	0.436
OXA5	9.8	5	0.524
OXO6 primary grains	3.4	3	0.629
particles	15	1.9	

Table 3
Specific surface area, apparent density and angle of repose of the metal powders obtained by reduction at 520 °C under hydrogen of the oxalic precursors

Metal powder	S_w (±0.05 m^2 g^{-1})	d_a (±0.001 g cm^{-3})	α (±1°)
OXA1R	0.93	0.590	48
OXA2R	0.71	0.630	46
OXA3R	0.82	0.740	40
OXA4R	0.85	0.850	Unmeasured, insufficient quantity of powder
OXA5R	0.95	0.890	41
OXO6R	0.72	1.110	42

which stabilize the metastable form. Indeed, Dzidziguri et al. [20] have stabilized the pure metastable cubic phase by synthesizing cobalt nanoparticles of about 30 nm in size.

The metallic cobalt content in the powders obtained by reduction at 520 °C of the oxalic precursors is about 99.9±0.1 wt.%. Whatever the studied sample is, the specific surface area (S_w) of the powder is approximately constant (0.7 to 1 m^2 g^{-1}, Table 3). The apparent density (d_a) and the angle of repose (α) of the metal powders are presented in Table 3.

SEM observations of the metal particles obtained from oxalic acid reveal a coralline morphology characterized by an entanglement of the original acicular particles (Fig. 3a–e). The medium size of the metal particles is about 50±0.5 µm, apart from the OXA2R powder (Fig. 3b) which presents a particles size of about 80±0.5 µm. The medium size of the primary grains is about 1±0.5 µm (Fig. 4a).

The shape of the OXO6R particles is approximately parallelepipedic, showing that the thermal decomposition of the starting oxalate is a pseudomorphous transformation (Fig. 3f). The measure of the average size of the metal cobalt particles was difficult, owing to an agglomeration of the particles during the reduction. These metal particles seems to be more compact (Fig. 4b) than those synthesized from oxalic acid (Fig. 4a).

An increase in the acicular ratio of the precursor particles issued from oxalic acid (Table 2) gives rise to a decrease in the apparent density of the metal powders (Table 3). A high value of the acicular ratio (about 15) probably favours the entanglement and disadvantages the agglomeration of the needles during the thermal decomposition. As shown by SEM observations, this phenomenon induces the formation of metal particles with a high porosity (Fig. 4a), an important shape irregularity and a strong surface roughness (Fig. 4c). It is assumed that a shape irregularity and a surface roughness hampers the particles rearrangement during the filling of a definite volume. Thus, these phenomena explain the lower value of apparent density obtained for these metal powders (about 0.6 g cm^{-3}). The value of the angle of repose of the OXA1R and OXA2R powders, upper than 45° (Table 3), agrees with the assumption that these metal powders present an important shape irregularity and a strong surface roughness. The values of α obtained for the OXA3R and OXA5R powders (40–41°) reveal that these samples present a higher ability to flow than OXA1R and OXA2R (46–48°) and therefore, a less important shape

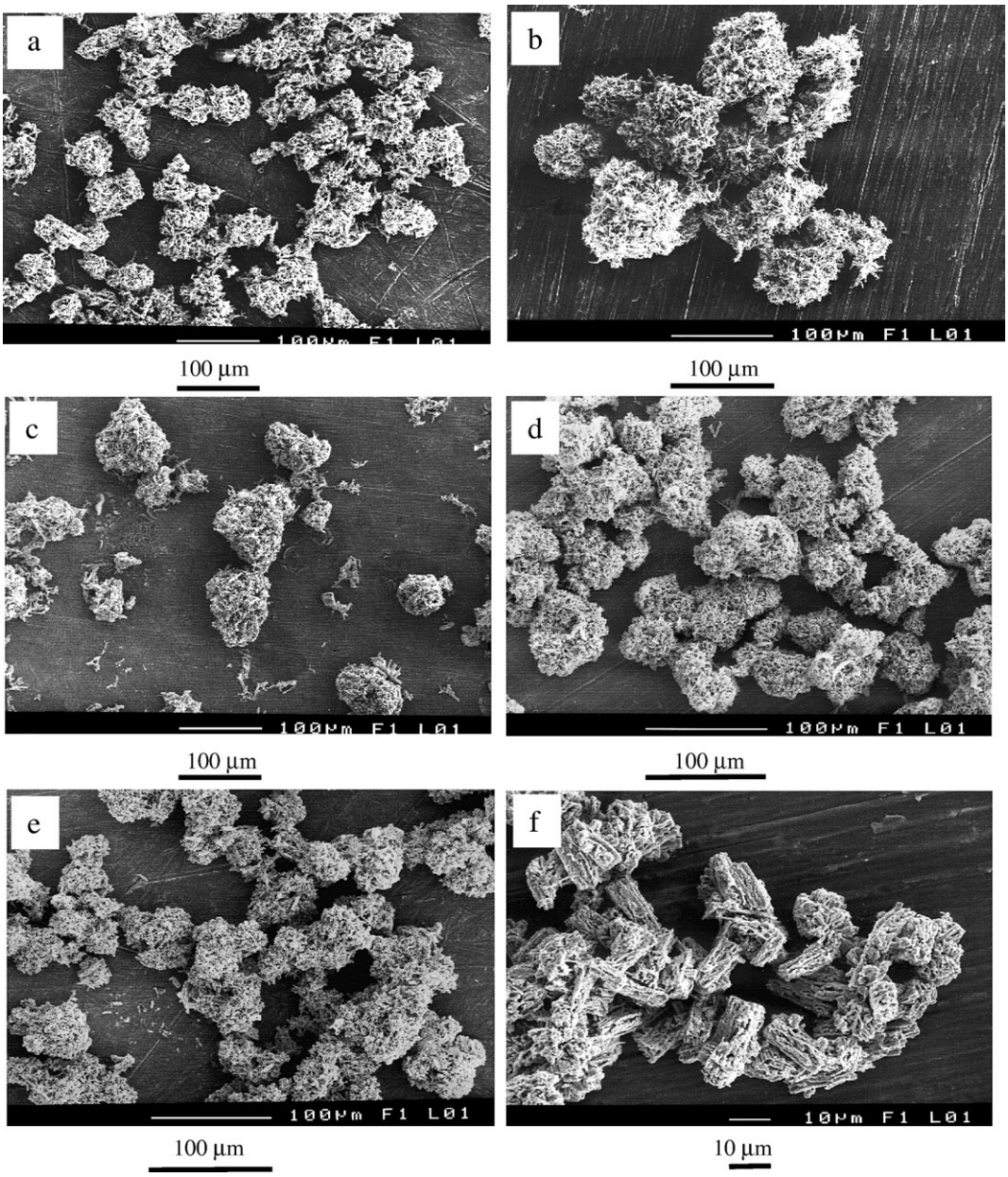

Fig. 3. SEM micrographs of the metal cobalt powders: (a) OXA1R; (b) OXA2R; (c) OXA3R; (d) OXA4R; (e) OXA5R; (f) OXO6R.

irregularity and a lower surface roughness of the particles. It results an increase in the apparent density of the metal powders (0.59 to 0.89 g cm^{-3}). The parallelepipedic particles, more regular in shape and more compact than the coralline particles (Figs. 3f and 4b), give rise to the higher value of apparent density (about 1.1 g cm^{-3}), due to a most compact packing of the particles during a gravitational filling.

To summarize, these results reveal that the synthesis of cobalt oxalate particles of high length (upper than 15 µm) and high acicular ratio (about 15) favours the preparation of metal cobalt powder with an important shape irregularity and a strong surface roughness. These final characteristics are related with a high angle of repose (>45°) and a low apparent density (about 0.6 g cm^{-3}).

4.3. Metal cobalt compacts

As revealed by the XRD patterns for all the compacts prepared, uniaxial pressing performed at 290 MPa on the metal cobalt powders gives rise to a partial transformation of the metastable fcc phase to the hcp stable phase. These results agree with those of Marinkovic et al. [21] which have shown that an increase in the compaction pressure from 100 to 1000 MPa induces a fcc to hcp cobalt phase transition. The ratio between the proportion of the cubic and hexagonal phases is then approximately the same whatever the studied compact is. Therefore, the influence of the cobalt structure on the mechanical properties of the compacts will be assumed identical for all the samples studied and will not be taken into account for the rest of the study.

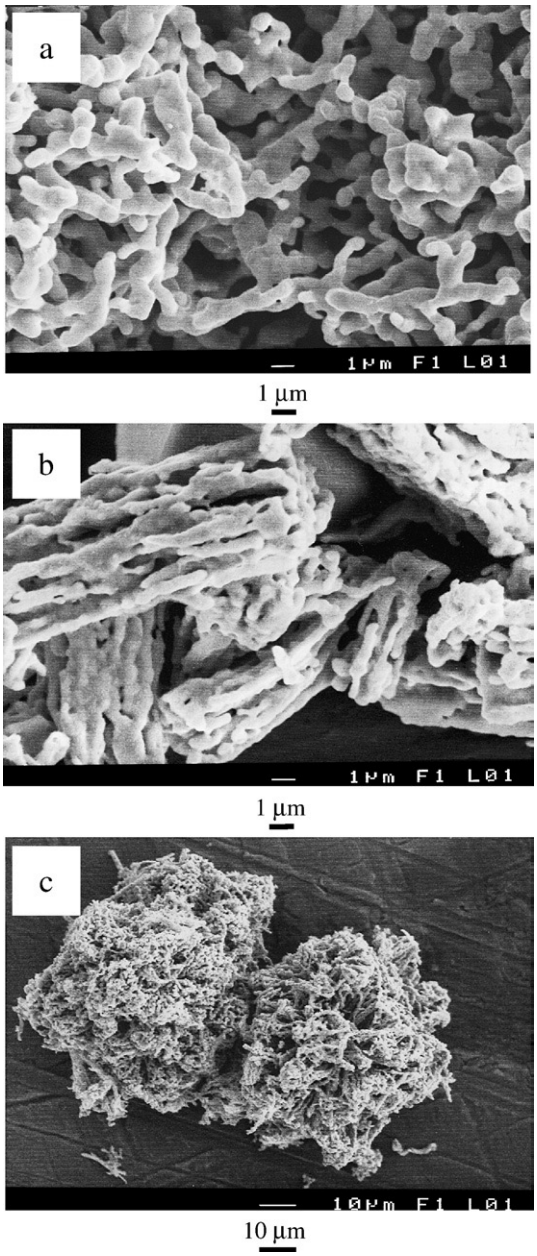

Fig. 4. SEM micrographs of the metal cobalt powders: (a) microstructure of the OXA1R coralline powder; (b) microstructure of the OXO6R parallelepipedic powder; (c) OXA1R coralline particles.

The bending strength up to the rupture (S) and the density (d) of the green metal compacts are presented in Table 4. The decrease in the green strength of the metal compacts from 47 MPa to 26 MPa could be related to the decrease in the density of the samples from 5.41 to 5.15 g. cm^{-3}. In order to reveal the real morphology influence on the bending strength, we have prepared two new green compacts from the OXA1R and OXO6R powders. Their density were adjusted to 5,38 g. cm^{-3} by tailoring the compaction pressure. The green strengths were equal to 42±3 MPa for OXA1RC and 24 MPa±3 MPa for OXO6RC.

This result confirms that the strength up to the rupture is mainly governed by the morphology of the metallic powders. Coralline cobalt particles are undoubtedly better to form highly strengthened green compacts than the parallelepipedic ones.

SEM observations of the surface of the metal compacts OXA1RC, OXA2RC, OXA3RC, OXA4RC and OXA5RC (Fig. 5a–e) reveal a strong overlapping of the adjacent filamentous grains during the compaction. Indeed, it appears difficult to identify single coralline particles after compaction.

In contrast, the parallelepipedic shape of the particles is still identifiable in the OXO6RC sample (Fig. 5f). No real particles entanglement is observed, making the cohesive forces very soft inside the green compact.

These phenomena allow to explain why a green metal cobalt compact (OXO6RC) composed of parallelepipedic particles presents lowest values of density and bending strength up to the rupture than green compacts made up of coralline particles (OXA1RC to OXA5RC).

After uniaxial compaction at 290 MPa, the density of OXO6RC (5.15 g cm^{-3}) is found lower than those of the coralline powders based compacts (5.26 to 5.41 g cm^{-3}). In the first stage of the compaction, corresponding to the rearrangement of the metal particles by interparticle sliding, the lower shape irregularity and surface roughness of the parallelepipedic powder let suppose a most compact packing than the coralline powders. Following the rearrangement stage, an increase in the compaction pressure gives rise to a more important densification of the coralline powder than that of the parallelepipedic powder because of a strong overlapping of the irregular shaped particles. These results agree with those of Poquillon et al. [12] performed on metal iron powders which have revealed that the original coralline morphology favours plastic deformations at the contact areas between the particles and gives rise to high green density level.

It is then assumed that the coralline morphology, characterized by an important intragranular porosity, a high shape irregularity and a strong surface roughness allows a great overlapping of the adjacent filamentous grains by plastic deformation during the compaction. As a result, a rigid metallic skeleton was formed and high values of bending green strength were obtained.

However, SEM micrographs of the studied coralline powder based compacts are quite similar (Fig. 5a–e) and could not explain the slight variation of density and green strength observed for these samples (Table 4). We can suppose that the decrease in the shape irregularity and surface roughness of the

Table 4
Green strength and density of the metal compacts obtained by compaction at 290 MPa of the corresponding metal powders

Metal compact	S (±3 MPa)	d (±0.05 g cm^{-3})
OXA1RC	47	5.41 (60.8%)
OXA2RC	45	5.41 (60.8%)
OXA3RC	43	5.30 (59.6%)
OXA4RC	38	5.27 (59.2%)
OXA5RC	37	5.26 (59.1%)
OXO6RC	26	5.15 (57.9%)

The percentages given in parentheses correspond to the ratio between the density of the metal compact and the density of pure metal cobalt equal to 8.9 g cm^{-3}.

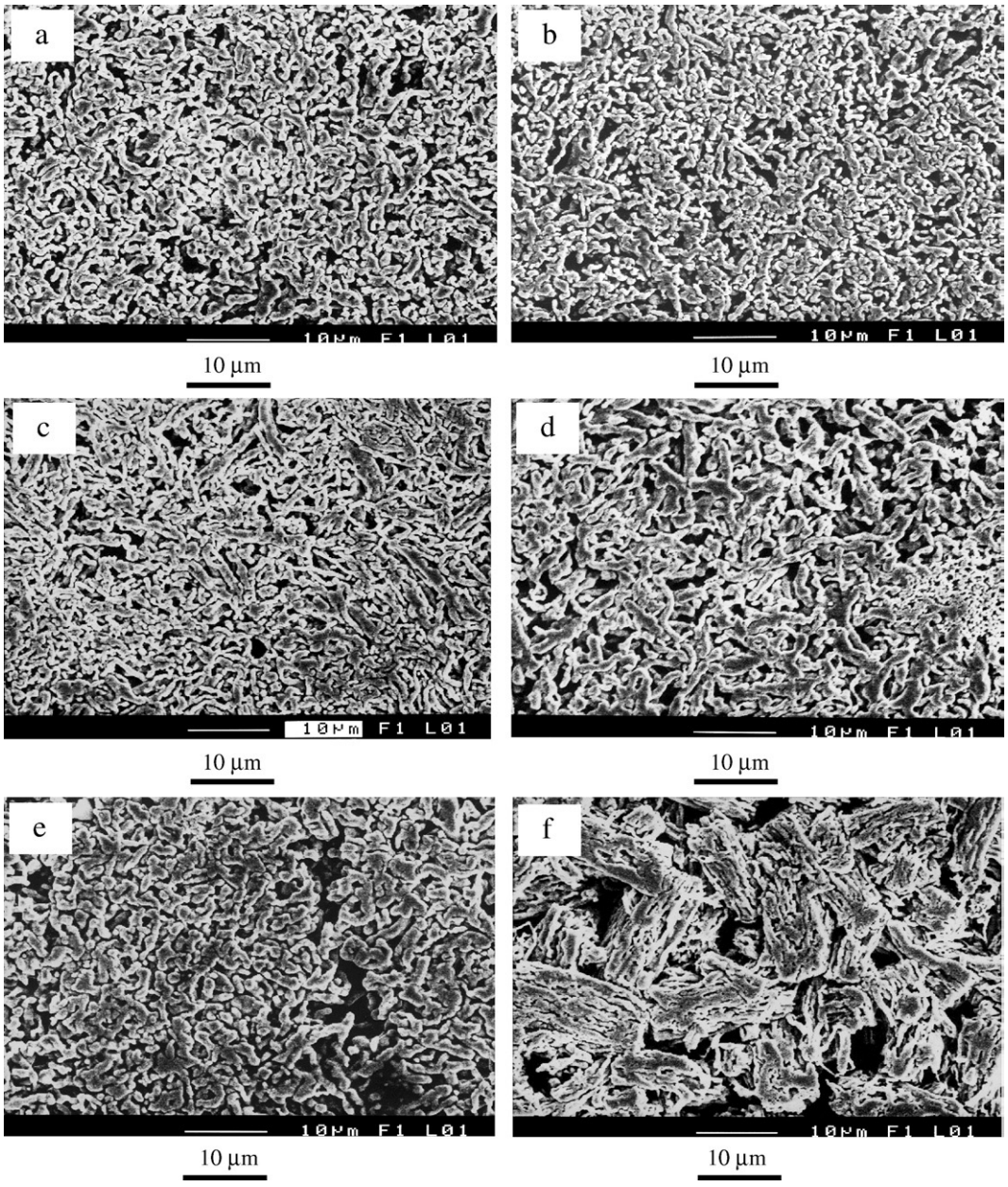

Fig. 5. SEM micrographs of the metal cobalt compacts: (a) OXA1RC; (b) OXA2RC; (c) OXA3RC; (d) OXA4RC; (e) OXA5RC; (f) OXO6RC.

coralline metal powders induced by a decrease in the acicular ratio of the precursor particles, gives rise to a decrease in the mechanical interlocking of the particles during the compaction.

5. Conclusion

Metal cobalt powders were synthesized by thermal decomposition under pure hydrogen of precipitated cobalt oxalates. Precipitation from oxalic acid gives rise to the formation of acicular particles in contrast to ammonium oxalate for which parallelepipedic particles were prepared. Coralline particles were obtained by an entanglement of the acicular particles during the reduction. In contrast, the parallelepipedic shape was conserved owing to a pseudomorphous thermal decomposition.

A strong length to diameter ratio favours the entanglement of the oxalate particles during a gravitational flow and disadvantages their agglomeration during thermal decomposition. Consequently, low values of apparent density have been obtained for oxalate and metal powders.

The coralline morphology, characterized by an important intragranular porosity, a high shape irregularity and a strong surface roughness allows a great overlapping of the adjacent filamentous grains during the compaction, in contrast to the parallelepipedic powder. The contact zones between the adjacent coralline particles are not local and involve a more important proportion of crystallites than in the case of the parallelepipedic particles. As a result, a rigid metallic skeleton was formed and high values of green density and bending green

strength up to the rupture were obtained (respectively, 60.8% and 47 MPa at $P_c = 290$ MPa).

References

[1] S. Roure, D. Bouvard, P. Dorémus, E. Pavier, Powder Metallurgy 42 (2) (1999) 164–170.
[2] O. Gillia, D. Bouvard, Materials Science and Engineering A 279 (2000) 185–191.
[3] L. Mao, Z. Shan, S. Yin, B. Liu, F. Wu, Journal of Alloys and Compounds 293–295 (1999) 825–828.
[4] Y. Liu, Y. Zhu, Y. Zhang, Y. Qian, M. Zhang, L. Yang, C. Wang, Journal of Materials Chemistry 7 (5) (1997) 787–789.
[5] P.J. James, Powder Metallurgy 1 (1977) 21–25.
[6] K. Kase, H. Yamamoto, Nippon Tungsten Review 12 (1979) 1–6.
[7] S.D. Strothers, K. Vedula, The International Journal of Powder Metallurgy 22 (4) (1986) 227–232.
[8] I.H. Moon, J.S. Choi, Powder Metallurgy 28 (1) (1985) 21–26.
[9] L.-P. Lefebvre, Y.-M. Henuset, Y. Deslandes, G. Pleizier, Powder Metallurgy 42 (4) (1999) 325–330.
[10] V. Baco-Carles, P. Combes, P. Tailhades, A. Rousset, Powder Metallurgy 45 (1) (2002) 33–38.
[11] P. Tailhades, V. Carles, A. Rousset, FR Patent N° 9907340 (1999) EUR Patent N° 00401628.3–2309 (2000) US Patent N° 6, 464, 750 B1 (2002).
[12] D. Poquillon, J. Lemaitre, V. Baco-Carles, Ph. Tailhades, J. Lacaze, Powder Technology 126 (2002) 65–74.
[13] ASM Handbook "Powder Metal Technologies and Applications", vol. 7, ASM International, Materials Park OH 44073–0002, ISBN: 0-87170-387-4, 1998, pp. 305–309.
[14] D. Poquillon, V. Baco-Carles, Ph. Tailhades, E. Andrieu, Powder Technology 126 (2002) 75–84.
[15] H. Pezerat, J. Dubernat, J.P. Lagier, Compte-Rendu de l'Académie des Sciences, Paris, France C 266 (1968) 1357–1360.
[16] R. Deyrieux, A. Peneloux, Bulletin de la Société Chimique de France 8 (1969) 2675–2681.
[17] J.P. Lagier, Ph. D. Thesis, Paris, France (1970).
[18] P. Tailhades, Ph. D. Thesis, Toulouse, France (1988).
[19] J.G. Parkhouse, A. Kelly, Proceeding of the Royal Society of London 451 (1943) (1995) 737–746.
[20] E.L. Dzidziguri, V.V. Levina, T.V. Samsonova, Russian Metallurgy 3 (1999) 102–105.
[21] B.A. Marinkovic, B.D. Stojanovic, Z. Rakocevic, A. Kremenovic, S. Duric, Crystal Research and Technology 34 (8) (1999) 1005–1010.